Effect of Macromolecular Architecture on the Morphology of Polystyrene–Polyisoprene Block Copolymers

ARTICLE *in* MACROMOLECULES · FEBRUARY 2013

Impact Factor: 5.8 · DOI: 10.1021/ma202650a

Macromolecules

Article

pubs.acs.org/Macromolecules

Effect of Macromolecular Architecture on the Morphology of Polystyrene–Polyisoprene Block Copolymers

C. Dyer,[†] P. Driva,[‡] S. W. Sides,[§] B. G. Sumpter,[⊥,#] J. W. Mays,[†,‡] J. Chen,[#] R. Kumar,[∥,⊥] M. Goswami,[⊥] and M. D. Dadmun*[,†,‡]

[†]Department of Chemistry, University of Tennessee, Knoxville, Tennessee 37996, United States

[‡]Chemical Sciences Division, Oak Ridge National Laboratory, Oak Ridge, Tennessee 37831, United States

[§]Tech-X Corporation, Boulder, Colorado 80303, United States

[∥]National Center for Computational Sciences, Oak Ridge National Laboratory, Oak Ridge, Tennessee 37831, United States

[⊥]Computer Science and Mathematics Division, Oak Ridge National Laboratory, Oak Ridge, Tennessee 37831, United States

[#]Center for Nanophase Materials Sciences, Oak Ridge National Laboratory, Oak Ridge, Tennessee 37831, United States

ABSTRACT: The impact of block connectivity on the morphologies of four block copolymers of varying architecture containing polystyrene (PS) and polyisoprene (PI) has been studied. The volume fraction of PS and molecular weight are held constant while varying the architecture from a linear PS–PI diblock copolymer to three different miktoarm star architectures: PS_2PI, $PSPI_2$, and PS_2PI_2. Morphologies of the PS_2PI and $PSPI_2$ miktoarm stars are different from those observed for the linear copolymer and dependent on the connectivity of the copolymer blocks. The change in morphology with connectivity indicates that combining two chains at a junction point leads to chain crowding, where subsequent excluded volume effects drive the change in morphology for each sample. The PS_2PI_2 miktoarm star exhibits the same morphology as the linear diblock but with a reduction in the size of the domains. The extent of the decrease in domain size indicates that chain stretching impacts the formation of this morphology. Experimentally observed morphologies for different chain architectures are generally consistent with three-dimensional self-consistent-field theory simulations, taking into account conformational asymmetry and experimental uncertainty in the copolymer composition. Furthermore, these results generally agree with analytical theory predictions that account for architectural and conformational asymmetry.

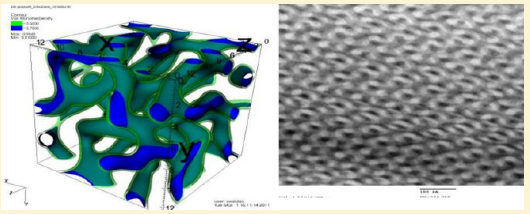

INTRODUCTION

For several decades, much attention has been focused on block copolymer materials, due largely to their ability to self-organize into a variety of morphologies having size features on the scale of nanometers.[1] The formation of these morphologies, typically spheres, cylinders, bicontinuous gyroid, and lamellae for two-component block copolymers,[2] is affected by a number of molecular characteristics such as molecular weight, molecular architecture, molecular structure, segregation strength, composition, and sample preparation. In general, morphological control of linear block copolymers is now well understood[3,4] and has led to useful applications of block copolymers as thermoplastic elastomers (TPEs)[5] and polymer blend compatibilizers.[6]

In contrast to the case for linear block copolymers, structure–morphology relationships for nonlinear block copolymers are much less explored, largely due, until recently, to a lack of synthetic methods for their tailored synthesis. In the 1970s, Bi and Fetters[7] synthesized and studied the morphologies and properties of star-block copolymers of polystyrene (PS) and polyisoprene (PI). Star-block copolymers are star polymers where each arm is itself a block copolymer, and these materials exhibited superior tensile strength relative to linear triblock copolymers having similar composition and molecular weights. Also in the 1970s, the synthesis of fairly well-defined multigraft copolymers having diene backbones and PS side chains was reported.[8,9] However, studies of the bulk morphology of these TPE materials were not described.

Beginning in the early 1990s, systematic studies aimed at elucidating the effect of branched architecture on the morphology and properties of block copolymers were initiated.[10] This work was made possible by the development of synthetic routes to well-defined miktoarm star architectures (chemically different arms linked together to form a star)[11−15] as well as to a variety of more complex branched block copolymer architectures.[16−20] Morphology studies on miktoarm stars indicate that macromolecular architecture can be used to tune morphology independent of the volume fraction of the two components.[21,22]

The morphological behavior of miktoarm stars, or more specifically "opposing polymer brushes", in the strong segregation limit has also been described in a theoretical study by Milner.[23] The Milner theory accounts for the fact that the A and B blocks may differ in conformational flexibility,

Received: November 20, 2012
Revised: February 5, 2013

   dx.doi.org/10.1021/ma202650a | Macromolecules XXXX, XXX, XXX–XXX

which will result in a variation in the stretching of the arms at the junction point. This computational result predicts morphologies of the miktoarm stars that are a function of the copolymer composition, φ_B (= 1 − φ_A), and molecular asymmetry, ε. Incorporating both architectural and conformational asymmetries, ε is calculated as $\varepsilon = (n_A/n_B)(l_A/l_B)^{1/2}$ where n_A and n_B are the numbers of A and B arms that are linked at the junction point and l_A and l_B are the conformational asymmetry parameters of the two-arm types. In particular, $l_i = 6v_i/b_i^2$ for i = A, B and v_i and b_i are the molar volume and the Kuhn segment length of block i, respectively. A general trend of this theory is that the block copolymer phase diagram exhibits a shift to a more curved morphology as the asymmetry factor, $\varepsilon > 1$, increases for a given copolymer composition for low B volume fraction copolymers.[23]

Preference for a curved morphology with an increase in the asymmetry parameter can be explained by the following argument. In the strong segregation limit, the interphase region between phases is about 2−5 nm.[24−26] Compared to the phase domain sizes, which are typically tens of nanometers, this interphase region is essentially a two-dimensional surface that has curvature properties that are correlated to the volume-filling characteristics of the blocks of the copolymer. As one moves from a convex to a concave curvature, the volume available to a polymer chain decreases. For a diblock copolymer, the magnitude of the interfacial curvature is proportional to the relative volumes available to the two blocks. Thus, the most asymmetric diblock copolymers form morphologies having the highest curvature, spheres. As the volume fraction of the two blocks becomes more comparable, the interfacial curvature decreases, and symmetrical diblock copolymers form a lamellar morphology with a flat interface. Similarly, there is a shift in interfacial curvature if there is architectural asymmetry at a junction point. For example, an A_2B miktoarm star copolymer exhibits architectural asymmetry, creating more lateral crowding and stretching on the side with the two A arms. Such architectural asymmetry has been found to promote the formation of morphologies that place the two A chains on the convex side of the interface.

Milner's theory has been tested experimentally, and the theoretically predicted shift of the morphological behavior with architectural asymmetry has been reported.[20,22] The agreement is encouraging but more studies are needed in order to fully understand the impact of macromolecular architecture on the morphology of nonlinear block copolymers. In previous experimental studies,[20,22] the molecular weight and volume fraction of a component vary among different samples. Such a variation among samples makes it hard to distinguish between the effects of conformational, architectural asymmetry, and composition changes.

In the present work, a series of PS−PI block copolymers were synthesized, holding copolymer composition (∼70 vol % PS) and molecular weight constant while varying copolymer architecture from a linear diblock copolymer to PS_2PI, $PSPI_2$, and PS_2PI_2 miktoarm stars. The morphologies of these block copolymers were characterized using transmission electron microscopy (TEM) and small-angle X-ray scattering (SAXS). The experimentally observed morphologies are also compared with those expected based on the Milner theory and self-consistent field theory in order to achieve a complete understanding of the factors that control the development of structure in block copolymers with changes in block connectivity.

EXPERIMENTAL SECTION

The four copolymers were synthesized using anionic polymerization and high-vacuum techniques in all glass reactors with break-seal transfers and sampling via constrictions.[27] The linear PS−PI copolymer was synthesized via sequential addition of styrene and isoprene according to standard anionic procedures.[28] The synthesis of PS_2PI, $PSPI_2$, and PS_2PI_2 miktoarm stars was conducted as described in the literature.[12−15,20] A portion of each arm was isolated and characterized prior to linking using chlorosilane chemistry. Excess arms used to drive the linking reaction to completion were removed by solvent/nonsolvent fractionation (toluene/methanol). A Polymer Laboratories PL-50 size exclusion chromatography (SEC) system, equipped with a Precision Detectors two-angle light scattering detector, was used to measure absolute molecular weights and polydispersity indices (PDI) of the polymers. The SEC system was operated in tetrahydrofuran (THF) at a flow rate of 1 mL/min. Refractive index increment (dn/dc) measurements were carried out in THF using a Wyatt Technology Optilab differential refractometer. Proton nuclear magnetic resonance (Bruker Avance 400 MHz wide-bore spectrometer, samples in d-$CHCl_3$) experiments were completed to determine the composition of the final fractionated copolymers.

For the TEM analysis, solid films ∼2 mm thick were cast from tetrahydrofuran solutions of 5 wt % polymer in 30 mL beakers. The evaporation of the solvent was controlled via small holes in aluminum foil covering the beaker and a larger beaker covering the 30 mL beaker in a fume hood, forming a solid film within 10−14 days. These films were then held for 2 days at room temperature and atmospheric pressure and then placed under vacuum to remove residual solvent. The vacuum oven temperature was ramped to 120 °C over the period of 3 days and kept there for 1 week. After annealing, the temperature was slowly ramped down to 80 °C over 2 days and then quickly lowered to room temperature. This casting and annealing procedure was designed to promote the development of equilibrium strongly segregated morphologies. The morphologies were determined using a Hitachi H800 tunneling electron microscope (TEM) at a voltage of 75 keV. The TEM samples were prepared by lowering the temperature of the sample to −90 °C and microtomed using a Boeckeler PowerTomeX UltraMicrotome. The slices were collected on a copper grid and stained with vapors from a 4% osmium tetroxide solution for 30 min.

The SAXS pattern for each sample was recorded on a Molecular Metrology small-angle X-ray instrument equipped with a two-dimensional position sensitive proportional detector of circular shape (radius = 2.5 cm), using Cu Kα radiation (λ = 1.5418 Å). A monochromatic X-ray source from the X-ray sealed tube is focused by a pair of Kirkpatrick−Baez microfocusing mirrors. The sample-to-detector distance was 1.5 m with the scattering vector (q) range of 0.01−0.15 $Å^{-1}$; $q = 4\pi/\lambda \sin(\theta/2)$, where λ is the X-ray wavelength and θ is the scattering angle.

SIMULATIONS

Numerical self-consistent field theory (SCFT) for dense polymer melts has been highly successful in describing complex morphologies in block copolymers.[29,30] In particular, the SCFT for the branched block copolymer melts is detailed in refs 30 and 31. The theory has been used recently to construct morphology diagrams for different kinds of miktoarm star copolymers.[32,33] Here, we only present a brief description of the numerical algorithms and relevant details related to comparison of the theory with the experiments.

The simulation method used in this study is the same as in ref 34. The copolymer chains containing A and B blocks are modeled as continuous curves. For comparison with the experimental system in this paper, the A and B species represent monomers of PS or PI, dependent on the sample. The chemical specificity of PS and PI is captured in the model through the value of the Flory parameter χ, which controls the

dx.doi.org/10.1021/ma202650a | Macromolecules XXXX, XXX, XXX−XXX

strength of the chain segregation that drives the formation of nanoscale morphologies.

After constructing a field theory using standard mathematical transformations,[30,31] the saddle-point approximation is invoked to obtain a set of nonlinear equations for the density and chemical potential fields of the system. The iterative algorithm described in ref 35 augmented with a "spectral filtering" algorithm[34,36] is used to find solutions for the SCFT equations. The filtering algorithm is used to get rid of topological defects[37] for large simulation sizes and is an improvement of the procedure described in ref 36. All the results presented in this work are obtained using the parallel framework implemented in the PolySwift++ code. Free energy of the bulk system is obtained by starting from different initial guesses for the densities and fields. These free energies are compared and the run with the lowest free energy value is chosen as the most likely space group that will be obtained in the experiments.

In order to compare the numerical results to experimental data, the PS−PI interaction energy scale must be matched to the SCFT simulation parameters. The energy scale in the theory is set by χN, N being the total number of Kuhn segments. For a similar system, the following temperature-dependent Flory−Huggins parameters for polyisoprene and polystyrene have been reported[38]

$$\chi_{IS}(T) = \frac{26.4}{T\,[^\circ\mathrm{C}] + 273.15} - 0.0287$$

based on a common segment volume of 118 Å^3. Using the annealing temperature of 120 °C gives an interaction parameter of $\chi = 0.0385$. Note that different temperature dependencies of the χ_{IS} are reported in the literature,[39,40] and this, in turn, hinders a quantitative comparison between the theory and experiments. However, a qualitative comparison is possible using these expressions. To estimate the number of segments, N, in the copolymer chains, the following homopolymer densities are used (at 140 °C):[38] $\rho_I = 0.830$ g/cm^3 and $\rho_S = 0.969$ g/cm^3 with an average molecular weight of $M_n = 100\,000$ Da. Using these parameters, we get a segregation strength of $\chi N = 54.0$. Very large segregation strengths can introduce numerical instabilities in the SCFT calculations. In order to improve the stability in the simulations, a lower value of $\chi N = 30.0$ is used. However, the well-known phase diagram for linear diblocks suggests that phase morphologies change little once the chains are strongly segregated. The SCFT simulations also account for the different Kuhn segment lengths for PS and PI. The values used in the simulation are taken from the literature[38] ($b_{PS} = 5.47$ Å and $b_{PI} = 6.07$ Å) and are based on a common segment volume of 118 Å^3 as mentioned above. Different values of b_{PS} and b_{PI} are used in the experimental analysis and are based on the polystyrene and polyisoprene repeat units (C8H8 and C5H8, respectively).[41]

RESULTS AND DISCUSSION

SEC chromatograms of the intermediate products during the synthesis of $PSPI_2$ are shown in Figure 1 and are typical and representative of those taken during the synthesis of all the block copolymers. The PS and PI arms were sampled and independently characterized for absolute weight-average molecular weights (M_w) and polydispersities prior to linking. The living PS arm was reacted with a ~100:1 excess of methyltrichlorosilane to create dichlorosilyl-terminated PS, where excess methyltrichlorosilane was removed from the

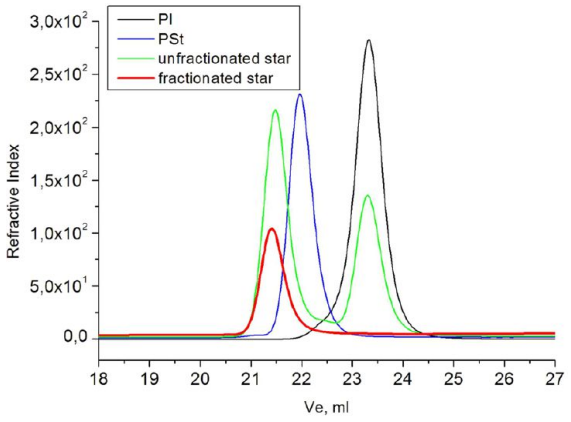

Figure 1. SEC chromatogram of the intermediate products in the synthesis of $PSPI_2$.

reactor by prolonged pumping on the vacuum line, and then reacted with excess living PI to create the miktoarm star. Excess PI was removed by fractionation, and the final product exhibits a narrow and symmetrical peak in SEC. The molecular characteristics of the precursor linear polymers and the final copolymers are provided in Table 1. Absolute M_w values were determined by SEC with light scattering detection, while the PDI values were determined based upon the SEC refractive index detector response. The weight percent values of PS in the block copolymer as determined by NMR, by light scattering (from M_w of the arms and the final block copolymers), and by refractive index increments (in THF) are listed in Table 1.

Table 2 lists the experimentally determined PS volume fractions of the four block copolymers based on the three different techniques: NMR spectroscopy, absolute molecular weight determinations, and dn/dc measurements (using the method described in ref 13). Clearly, all four block copolymers are quite similar in composition. Good agreement, within a few percent, is observed for the measured compositions of a given sample by the different techniques.

The morphologies of the copolymers are characterized by TEM and SAXS, where the SAXS data are displayed as the circularly averaged, one-dimensional plots of intensity (I) in absolute units (cm^{-1}) as a function of q. q^* in each plot is defined as the scattering vector of the primary Bragg peak, and q_n are the series of higher order peaks. Each of the SAXS patterns includes points that denote the expected position of higher order peaks for the preliminarily assigned morphology. The q^* values for the PS-b-PI, $PSPI_2$, PS_2PI, and PS_2PI_2 were found to be 0.0115, 0.0145, 0.0146, and 0.0142 Å^{-1}, respectively, corresponding to a d-spacing ($q^* = 2\pi/d$) of 54, 43, 43, and 44 nm, respectively.

A TEM image of the PS-b-PI sample is presented in Figure 2. A brief inspection of this figure may lead to an initial assignment of a lamellar morphology. However, upon closer inspection, the polyisoprene domains (dark lines) appear to be narrower than the polystyrene domains (lighter lines), which is consistent with the projection of hexagonally packed cylinders that are cut along the tube axis, but not lamellae. SAXS data provide additional insight, as shown in Figure 3, where the ratios of the peak positions of higher order peaks to that of the primary peak are shown. The SAXS data clearly indicate that this diblock copolymer exhibits a hexagonally close-packed cylindrical (HCPC) morphology. This result is in accord with the expected morphology for a PS−PI diblock copolymer of

dx.doi.org/10.1021/ma202650a | Macromolecules XXXX, XXX, XXX−XXX

Table 1. Molecular Characteristics of Precursor Homopolymers and Final PS−PI Block Copolymers

sample	M_w PS[a] arm (kg/mol)	M_w PI[a] arm (kg/mol)	M_w final[a] (kg/mol)	PDI final[b] (M_w/M_n)	wt % PS (NMR)	wt % PS (LS)	dn/dc_{exp}	dn/dc_{calc}
PS−PI	70.9		104.1	1.06	71	68	0.1691	0.168
PS_2PI	32.1	27.5	90.3	1.06	69	70	0.1697	0.169
$PSPI_2$	73.4	16.2	104.4	1.05	73	70	0.1696	0.169
PS_2PI_2	36.4	17.4	105.9	1.07	70	68		0.168

[a]Via SEC-LS. [b]Via SEC-DRI.

Table 2. Volume Fractions of the Block Copolymers As Determined by Various Characterization Techniques

sample	φ_{PS} NMR	φ_{PS} LS with calcd dn/dc	φ_{PS} from measd dn/dc
PS−PI	0.71	0.66	0.67
PS_2PI	0.65	0.67	0.68
$PSPI_2$	0.70	0.66	0.68
PS_2PI_2	0.67	0.65	

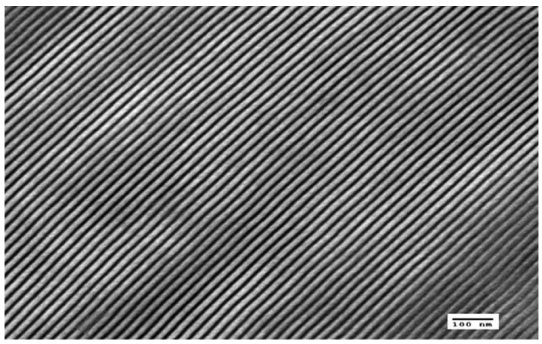

Figure 2. TEM of the linear PS-*b*-PI copolymer.

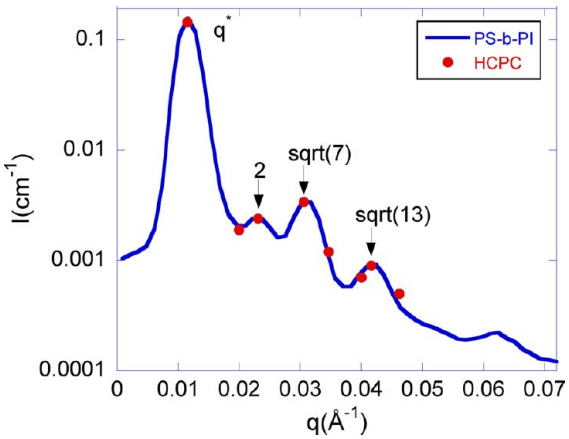

Figure 3. SAXS curve of the linear PS-*b*-PI copolymer plotted with peaks that are expected for the HCPC morphology.

0.68 volume fraction PS—the composition that represents the average of the three values reported in Table 2.[2] The numerical SCFT results for the PS−PI diblock (Figure 4) also clearly show hexagonally packed cylinders for 0.70/0.30 PS/PI linear diblock copolymer. Therefore, all experimental and computational studies clearly demonstrate that the PS−PI linear diblock synthesized for this study forms the expected cylindrical morphology.

The structure of the PS_2PI_2 miktoarm copolymer can be thought of as two linear diblock copolymers that are joined at their junction points but are half the length of the original diblock. Based on this picture and its architectural symmetry, the morphology of this copolymer should mimic that of the PS-

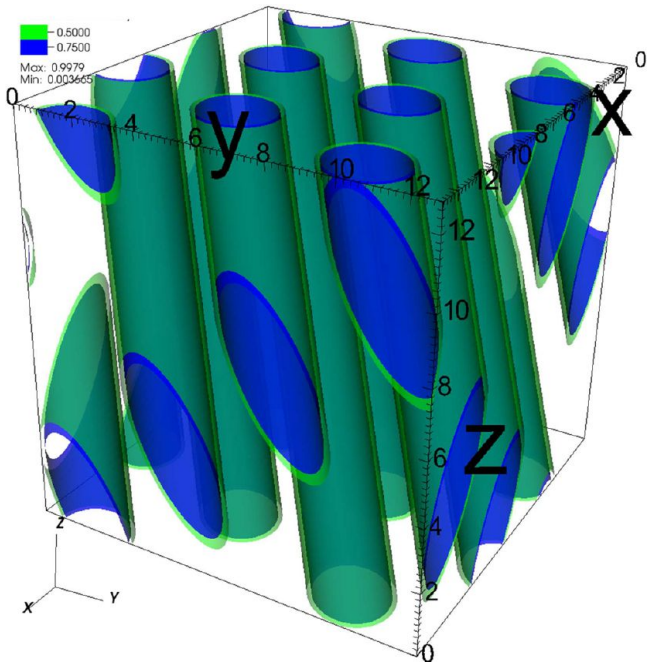

Figure 4. Density contours from numerical SCFT simulation of PS−PI diblock in bulk (PS volume fraction = 0.70, PI volume fraction = 0.30). Spectral filtering is turned on, and the results shown are for the lowest free energy among all runs performed on this sample.

b-PI linear diblock. The TEM images of this sample, examples of which are shown in Figure 5a,b, exhibit structures that are consistent with a cylindrical morphology. The SAXS results, shown in Figure 6, verify the assignment of this morphology as cylindrical.

As mentioned above, the 4-arm star can be envisioned as approximating a linear diblock copolymer that is half the length, as both the PS block and PI block of the PS_2PI_2 are one-half the length of the PS−PI copolymer. If this decrease in molecular weight were the only factor governing the phase domain structure, the domain size of the PS_2PI_2 should be 63% ($D \sim N^{2/3}$) of the PS−PI diblock. Analysis of the SAXS data, however, indicates that the PS_2PI_2 domain size is 10 nm (44 nm vs 54 nm) smaller than that of the PS-*b*-PI domain size, a decrease of 18%.

The SCFT simulation result is in good agreement with experiment for the PS-*b*-PI (~46 nm) though it underestimates the domain spacing in the PS_2PI_2 (~23 nm). A possible reason is the uncertainty in the estimation of the χN used in the SCFT calculation. Clearly the experimentally determined domain spacing of the 4-arm miktoarm star copolymer indicates that the connectivity of the blocks dramatically impacts the stretching of the blocks. In the 4-arm star, there exist two chains packed in each domain near one junction point. The result of excluded volume in this region is that each arm must extend away from the junction point significantly. This chain

dx.doi.org/10.1021/ma202650a | Macromolecules XXXX, XXX, XXX−XXX

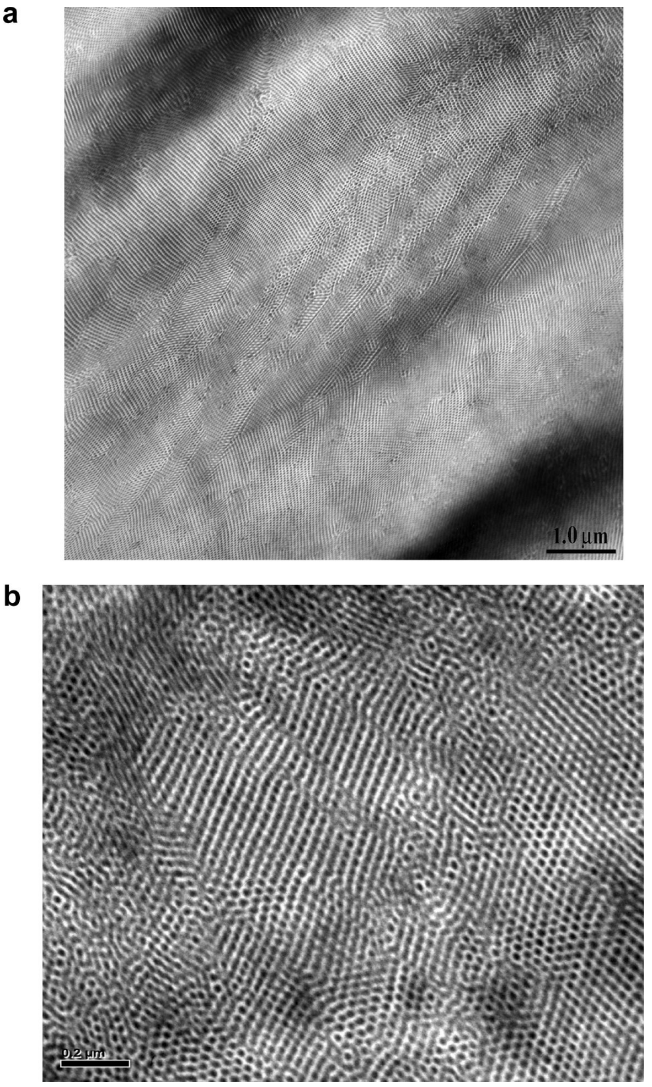

Figure 5. (a) TEM images of the PS_2PI_2 miktoarm star, exhibiting features that are consistent with a cylindrical morphology. (b) Different projection of the PS_2PI_2 miktoarm star, exhibiting features that are consistent with a cylindrical morphology.

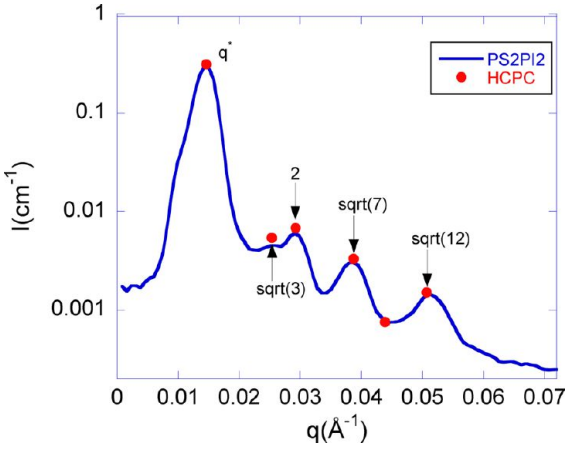

Figure 6. Small-angle X-ray curve of the PS_2PI_2 miktoarm star plotted with peaks expected for HCPC morphology.

stretching near the junction point dominates the chain conformation, resulting in a domain size for the PS_2PI_2 miktoarm star that is significantly larger than 63% of the linear PS-*b*-PI domain size.

An understanding of the role of asymmetric chain connectivity on the copolymer morphology can be gleaned by comparing these two cylindrical morphologies to those of the PS_2PI and $PSPI_2$ branched block copolymers. Multiple TEM images of the PS_2PI sample exhibit the morphological characteristics of body centered cubic (BCC) spheres. An exemplary image of the PS_2PI sample is shown in Figure 7,

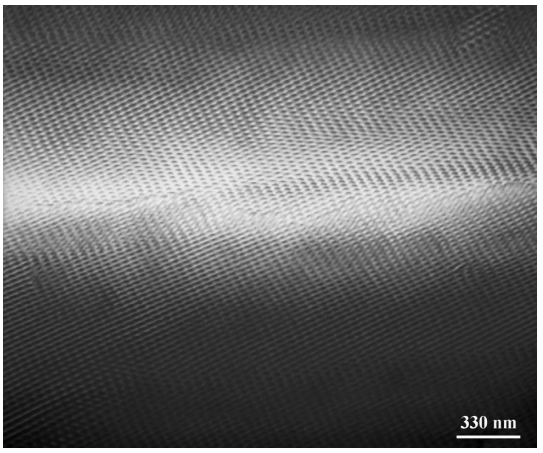

Figure 7. A representative TEM image of the PS_2PI miktoarm star copolymer.

where the PI chains (dark phase) form the spheres in this sample, and the matrix is composed of the PS component. Thus, placing the junction point between components in the middle of the PS block, rather than the end, results in the formation of a morphology with higher curvature, spheres. The high curvature of this morphology is a result of the requirement that two PS arms be connected to the junction point and pack into the domain. This packing of relatively rigid PS arms requires significant surface area, which in turn results in a highly curved spherical morphology.

Electron microscopy (Figure 8A,B) clearly shows that the $PS-PI_2$ copolymer exhibits the gyroid morphology. Thus, placing the junction point in the middle of the (more flexible) PI block results in a morphology with lower curvature (gyroid vs cylinder). This again is driven by the packing requirement of the two PI arms, which must be connected at the junction point. However the shorter, more flexible PI arms require less surface area than the longer PI arm of the linear diblock, which results in the lower curvature morphology.

Comparison between Experimental and Computational Results. Comparison of the computational and experimental results provides additional insight into the fundamental driving forces that control the observed morphology of these architecturally dissimilar block copolymers. The simulations are in qualitative agreement with the experimental results for the PS_2-PI and $PS-PI_2$ samples but are not as conclusive as the more precise correlation that exists between computation and experiment for the PS_2-PI_2 and linear PS−PI samples. Figure 4 shows the density contours for the PS-*b*-PI linear diblock system from numerical SCFT simulations for Φ_{PS} = 70%. Experimental results show that this sample forms hexagonal cylinders, as expected from numerous theoretical treatments and other SCFT calculations. Figure 9 shows the density contours for the PS_2-PI_2 sample from

dx.doi.org/10.1021/ma202650a | *Macromolecules* XXXX, XXX, XXX−XXX

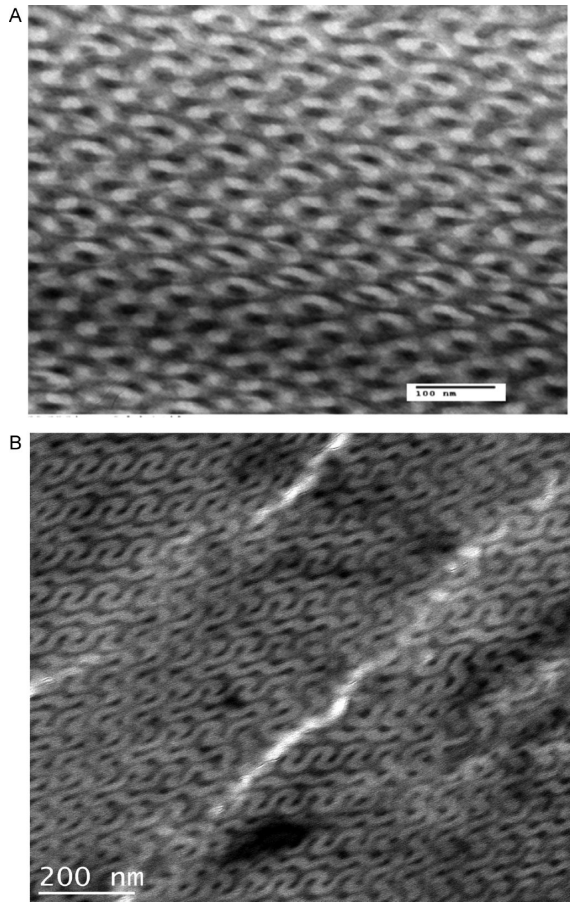

Figure 8. (A) TEM image of the $PSPI_2$ miktoarm star copolymer exhibiting the characteristic patterns of the gyroid morphology. (B) Different projection of the $PSPI_2$ miktoarm star copolymer sample.

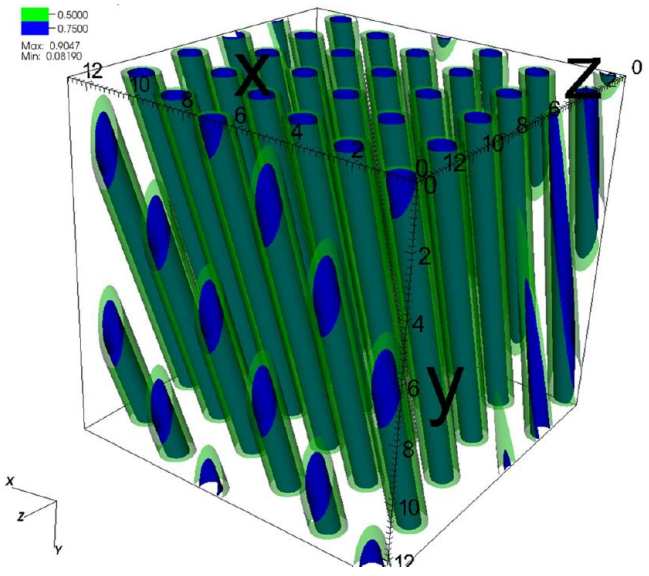

Figure 9. Density contours from numerical SCFT simulation of the PS_2–PI_2 diblock in bulk (PS volume fraction = 0.70, PI volume fraction = 0.30). Spectral filtering is turned on, and the results shown are for the lowest free energy among all runs performed on this sample.

numerical SCFT simulations for Φ_{PS} = 70%, where the experimental results also exhibit hexagonal cylinders, in good agreement with the simulations. In addition, the domain size of the cylinders in PS_2PI_2 decreased relative to those in the PS–PI linear diblocks, also in qualitative agreement with experiment. Additional SCFT simulations on the PS_2–PI_2 sample were completed, where the segregation strength and PS volume fraction were varied. These calculations also showed the formation of hexagonal cylinder morphologies, indicating this PS_2–PI_2 system is well within the hexagonal cylinder region of the phase diagram.

Figure 10A shows the density contours for the PS–PI_2 system from numerical SCFT simulations for Φ_{PS} = 74% with spectral filtering turned off. NMR results show that Φ_{PS} is higher in this sample than the other branched structures; therefore, the SCFT simulations for this sample are performed for a Φ_{PS} of 74. These results are consistent with a bicontinuous gyroid morpology with defects, which agrees with the TEM and SAXS results. Similarly, Figure 10B shows the density contours for the PS–PI_2 system from numerical SCFT for Φ_{PS} = 74% and with spectral filtering turned on. This cylindrical morphology represents the morphology for this sample with the lowest free energy. In fact, the free energies of the two morphologies in Figure 10A,B are within a few percent. The similarities of the free energies of these two morphologies are consistent with the conclusion that this specific PS–PI_2 sample is very close to the hexagonal cylinder/gyroid phase boundary. The experimental system naturally has additional sources of variability (polydispersity, kinetic effects, etc.) that cause the results to be pushed into the bicontinuous gyroid phase rather than the hexagonal cylinder phase.

Figure 11A shows density contours for the PS_2–PI system from numerical SCFT for Φ_{PS} = 70% and with spectral filtering turned on, while Figure 11B shows the density contours of the PS_2–PI with spectral filtering turned off. The well-ordered BCC phase shown in Figure 11A does not have the lowest free energy for the simulation runs; however, the free energy is extremely close to that of the simulation shown in Figure 11B. Additionally, the domains of the minor phase in Figure 11B are roughly spherical as well, indicating that the PI domains in the PS_2–PI copolymer will tend to form spheres. As in the PI_2–PS copolymer, the real polymer contains additional variability not captured in the SCFT calculation, and therefore this computational result can provide insight and direction in defining the equilibrium morphology of branched block copolymers but does not precisely define the equilibrium morphology.

Thus, these results indicate that the incorporation of branched junctions in block copolymers alters the packing of the blocks and shifts the phase boundaries in the resultant block copolymer. The results presented here offer insight into the detailed role this change in architecture has on the packing of the blocks and therefore polymer chains into microphase-separated structures. The linear diblock copolymer in this study forms a cylindrical morphology, while the branched copolymers form cylindrical (PS_2PI_2), spherical (PS_2PI), and gyroid ($PSPI_2$) morphologies. The alteration in morphology with block connectivity is interpreted to be the result of the packing of the branched rigid or flexible blocks that are confined to a junction point. This local packing constraint leads to an increase in curvature with the packing of the rigid chains at the junction in the matrix or a decrease in curvature with the packing of the more flexible chains in the minor phase.

Table 3 shows a summary of the results of this study. This table shows general agreement between our experimental results, SCFT computational studies, and previously reported

dx.doi.org/10.1021/ma202650a | *Macromolecules* XXXX, XXX, XXX–XXX

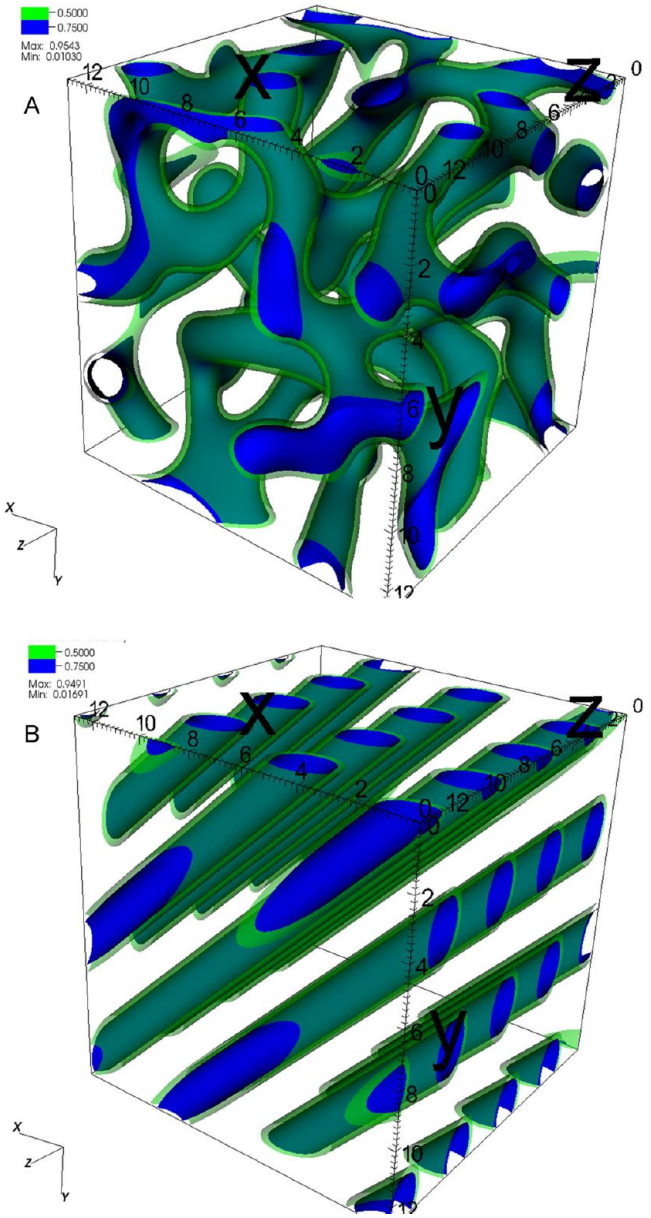

Figure 10. (A) Density contours from numerical SCFT simulation of $PS-PI_2$ diblock in bulk (PS volume fraction = 0.74, PI volume fraction = 0.26). Spectral filtering is turned off, and the morphology is not completely ordered. While the free energy of this configuration is not the lowest among all the spectral filtering runs, it is within a few percent of the lowest free energy value obtained in (B). This configuration is consistent with a gyroid morphology with defects. (B) Density contours from numerical SCFT simulation of $PS-PI_2$ diblock in bulk (PS volume fraction = 0.74 PI, volume fraction = 0.26). Spectral filtering is turned on and shows the most well-ordered morphology obtained, and the free energy of this configuration is the lowest among all the different simulations runs. Since the free energy values for all of the spectral filtering runs are within a few percent, this suggests that the parameters for this $PS-PI_2$ copolymer place the system near a morphological phase boundary.

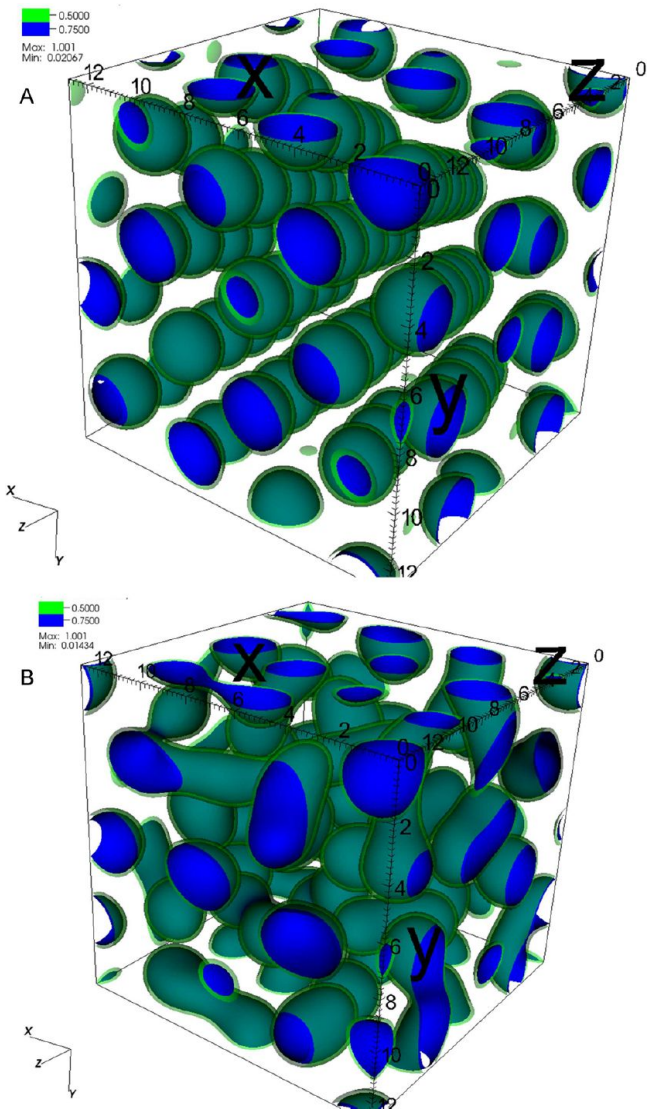

Figure 11. (A) Density contours from numerical SCFT simulation of PS_2-PI diblock in bulk (PS volume fraction = 0.70, PI volume fraction = 0.30). Spectral filtering is turned on and shows well-ordered spheres. While this does not represent the lowest free energy state, it is within a few percent of the free energy value in (B). (B) Density contours from numerical SCFT simulation of PS_2-PI diblock in bulk (PS volume fraction = 0.70, PI volume fraction = 0.30). Spectral filtering is turned off and shows spherical-like domains. The free energy is the lowest for this simulation and within a few percent of the free energy in (A).

Table 3. Morphologies Observed for the Four PS–PI block Copolymers[a]

	expt	SCFT	Milner's theory
PS-*b*-PI	HCPC	HCPC	HCPC
PS_2-PI	spheres	spheres	spheres
$PS-PI_2$	gyroid	gyroid	lamellar
PS_2-PI_2	HCPC	HCPC	HCPC

[a]HCPC is hexagonally close-packed cylinders.

theoretical work.[23] To compare to previous theoretical work, the architectural asymmetry parameter, $\varepsilon = (n_A/n_B)(l_A/l_B)^{1/2}$, is calculated. For the calculations, we have used v_{PS} = 176 Å^3, v_{PI} = 132 Å^3, b_{PS} = 6.9 Å, and b_{PI} = 6.8 Å.[41] One discrepancy lies in the $PS-PI_2$ results, where a cocontinuous morphology is observed experimentally and corroborated by SCFT calculations; however, the Milner theory predicts a lamellar morphology. It should be pointed out, however, that the theory qualitatively agrees with the experimental findings in that it predicts a morphology with decreased curvature, consistent with the result reported here. The origin of this

dx.doi.org/10.1021/ma202650a | *Macromolecules* XXXX, XXX, XXX–XXX

discrepancy lies in the use of round unit-cell approximation by Milner, which gives lower bound for the free energy.[31] In contrast, the free energy in the SCFT is computed exactly without resorting to any such approximations. An underestimation of the free energy leads to the prediction of a lower curvature morphology (lamellar). However, gyroid was experimentally observed indicating that the two PI chains are able to take an entropic penalty by stretching out in order to minimize excluded volume interactions. This entropic penalty appears to be favored over a greater enthalpic penalty that would result from the formation of the lower curvature lamellar morphology.

Note that the effects of conformational asymmetry have been largely ignored in the previous SCFT studies[31−33,42] on nonlinear block copolymers. It is very well-known that conformational asymmetry[43−48] plays a significant role in affecting the disorder−order and order−order transition boundaries in the case of linear block copolymer melts. However, it is not clear how the conformational asymmetry affects the boundaries in the weak and intermediate segregation limit for nonlinear block copolymers, which is of relevance to our experimental work. This limitation of the published works has motivated us to use SCFT *with conformational asymmetry,* which is more realistic. Excellent agreement between our SCFT calculations and experiments is found.

In the end, we compare our experimental and real-space SCFT results with other theoretical studies on nonlinear block copolymers published in the literature. In particular, work by Grason et al.[31,42] and Matsen[32] focused on the construction of morphology diagrams for conformationally symmetric nonlinear block copolymers using spectral methods.[30] Quantitative comparison of our experimental results to Figure 2 in ref 42 and Figure 5 in ref 32 shows discrepancies. A similar real-space SCFT study[33] for conformationally symmetric nonlinear block copolymers shows the same. In particular, for an estimated value of χN = 54 for the $PSPI_2$ molecules studied by us, all of these studies predict a lamellar morphology (even for Φ_{PS} = 74%), while experimentally, a gyroid morphology is found. For a reduced value of χN = 30, used in our SCFT calculations, an excellent agreement with these studies is observed, and the sample is found to be close to the cylinder−gyroid boundary. Similarly, the PS_2PI sample at χN = 30 and Φ_{PS} = 70% is predicted[32,33,42] to be close to the sphere−cylinder boundary. Our SCFT calculations incorporating conformational asymmetry as presented in Figure 11 show elongated spheres, which confirm qualitative agreement with these previous studies. Observed qualitative agreement between our calculations and the SCFT studies for conformationally symmetric miktoarm block copolymers are an outcome of the small conformational asymmetry parameter between polystyrene and polyisoprene pair.

CONCLUSIONS

Experimental and computational results are reported that document the effect of block connectivity on the morphology of four block copolymers consisting of styrene and isoprene, where generally good agreement is found. The reported results indicate that the excluded volume of packing multiple blocks into a domain at a junction point dominates the formation of the resultant morphologies. For instance, introducing a branch point in the majority (PS) block (i.e., the PS_2−PI copolymer) leads to the formation of a spherical morphology, whereas the linear PS−PI diblock copolymer exhibits a cylindrical morphology. The formation of this higher curvature morphology is the result of packing two PS chains into the matrix at a single junction point. Similarly, the introduction of a branch point in the flexible minor phase (PS−PI_2) leads to the formation of the gyroid morphology, which is the consequence of packing two PI chains into the minor phase to form a lower curvature morphology. Therefore, the formation of the new morphology is governed by the minimization of chain crowding at the junction point. The morphology of the four-arm star follows this trend, in that the size of the domain is dominated by the excluded volume of the chain pairs on each side of the interphase, resulting in significant chain stretching that minimizes the domain size reduction that results from smaller block lengths.

AUTHOR INFORMATION

Corresponding Author

*E-mail dad@utk.edu.

Notes

The authors declare no competing financial interest.

ACKNOWLEDGMENTS

This research is supported by the Department of Energy, Office of Basic Energy Sciences, Division of Materials Sciences and Engineering. We also acknowledge and thank A. Avgeropoulos for help with TEM. J. Chen acknowledges support from the Center for Nanophase Materials Sciences, which is sponsored by the Scientific User Facilities Division of DOE. Some of the computations used resources of the Oak Ridge Leadership Computing Facility at the ORNL

REFERENCES

(1) *Block Copolymers: Synthetic Strategies, Physical Properties, and Applications*; Hadjichristidis, N., Pispas, S., Floudas, G., Eds.; John Wiley: Hoboken, NJ, 2003.
(2) Bates, F. S.; Fredrickson, G. H. *Annu. Rev. Phys. Chem.* **1990**, *41*, 525.
(3) Russell, T. P. *Curr. Opin. Colloid Interface Sci.* **1996**, *1*, 107.
(4) Bates, F. S.; Fredrickson, G. H. *Phys. Today* **1999**, *52*, 32.
(5) Legge, N. R., Holden, G., Schroeder, H. E., Eds.; *Thermoplastic Elastomers*; Hanser: Munich, 1987.
(6) Anastasiadis, S. H.; Gancarz, I.; Koberstein, J. T. *Macromolecules* **1989**, *22*, 1449. Eastwood, E. A.; Dadmun, M. D. *Macromolecules* **2002**, *35*, 5069. Macosko, C. W.; Guegan, P.; Khandpur, A. K.; Nakayama, A.; Marechal, P.; Inoue, T. *Macromolecules* **1996**, *29*, 5590.
(7) Bi, L. K.; Fetters, L. J. *Macromolecules* **1976**, *9*, 732.
(8) Falk, J. C.; Schlott, R. J.; Hoeg, D. F.; Pendleton, J. F. *Rubber Chem. Technol.* **1973**, *46*, 1044.
(9) Hadjichristidis, N.; Roovers, J. *J. Polym. Sci., Polym. Phys. Ed.* **1978**, *16*, 851.
(10) Pitsikalis, M.; Pispas, S.; Mays, J. W.; Hadjichristidis, N. *Adv. Polym. Sci.* **1998**, *135*, 1.
(11) Hadjichristidis, N.; Iatrou, H.; Pitsikalis, M.; Mays, J. W. *Prog. Polym. Sci.* **2006**, *31*, 1068.
(12) Mays, J. W. *Polym. Bull.* **1990**, *23*, 247.
(13) Iatrou, H.; Hadjichristidis, N. *Macromolecules* **1992**, *25*, 4649.
(14) Iatrou, H.; Hadjichristidis, N. *Macromolecules* **1993**, *26*, 2479.
(15) Iatrou, H.; Siakali-Kioulafa, E.; Hadjichristidis, N.; Roovers, J.; Mays, J. W. *J. Polym. Sci., Polym. Phys. Ed.* **1995**, *33*, 1925.
(16) Pispas, S.; Mays, J. W.; Pochan, D.; Gido, S. P.; Hadjichristidis, N. *Macromolecules* **1996**, *29*, 7022.
(17) Lee, C.; Gido, S. P.; Poulos, Y.; Hadjichristidis, N.; Beck Tan, N.; Trevino, S. F.; Mays, J. W. *J. Chem. Phys.* **1997**, *107*, 6460.
(18) Lee, C.; Gido, S. P.; Pitsikalis, M.; Mays, J. W.; Beck Tan, N.; Trevino, S.; Hadjichristidis, N. *Macromolecules* **1997**, *30*, 3732.

(19) Lee, C.; Gido, S. P.; Poulos, Y.; Hadjichristidis, N.; Beck Tan, N.; Trevino, S. F.; Mays, J. W. *Polymer* **1998**, *39*, 4631.
(20) Beyer, F. L.; Gido, S. P.; Buschl, C.; Iatrou, H.; Uhrig, D.; Mays, J. W.; Chang, M. Y.; Garetz, B. A.; Balsara, N. P.; Beck Tan, N.; Hadjichristidis, N. *Macromolecules* **2000**, *33*, 2039.
(21) Hadjichristidis, N.; Iatrou, H.; Behal, S. K.; Chludzinski, J. J.; Disko, M. M.; Garner, R. T.; Liang, K. S.; Lohse, D. J.; Milner, S. T. *Macromolecules* **1993**, *26*, 5812.
(22) Pochan, D. J.; Gido, S. P.; Pispas, S.; Mays, J. W.; Ryan, A. J.; Fairclough, P.; Terrill, N.; Hamley, I. W. *Macromolecules* **1996**, *29*, 5091.
(23) Milner, S. T. *Macromolecules* **1994**, *27*, 2333.
(24) Hashimoto, T.; Todo, A.; Itoi, H.; Kawai, H. *Macromolecules* **1977**, *10*, 377.
(25) Helfand, E.; Wasserman, Z. R. *Macromolecules* **1976**, *9*, 879.
(26) Bates, F. S.; Berney, C. V.; Cohen, R. E. *Macromolecules* **1983**, *16*, 1101.
(27) Uhrig, D.; Mays, J. W. *J. Polym. Sci., Part A: Polym. Chem.* **2005**, *43*, 6179.
(28) Hadjichristidis, N.; Iatrou, H.; Pispas, S.; Pitsikalis, M. *J. Polym. Sci., Part A: Polym. Chem.* **2000**, *38*, 3211.
(29) Fredrickson, G. H.; Ganesan, V.; Drolet, F. *Macromolecules* **2002**, *35*, 16.
(30) Fredrickson, G. H. *The Equilibrium Theory of Inhomogeneous Polymers*; Oxford University Press: New York, 2006.
(31) Grason, G. M. *Phys. Rep.* **2008**, *433*, 1−64.
(32) Matsen, M. W. *Macromolecules* **2012**, *45*, 2161.
(33) Kumar, R.; Li, Y.; Sides, S. W.; Mays, J. W.; Sumpter, B. G. *J. Phys.: Conf. Ser.* **2012**, *402*, 012042.
(34) Zhang, J.; Sides, S. W.; Bates, F. S. *Macromolecules* **2012**, *45*, 256.
(35) Sides, S. W.; Fredrickson, G. H. *Polymer* **2003**, *44*, 5859.
(36) Bosse, A. W.; Sides, S. W.; Katsov, K.; Garcia-Cervera, C. J.; Fredrickson, G. H. *J. Polym. Sci., Part B: Polym. Phys.* **2006**, *18*, 2495.
(37) Hammond, M. R.; Sides, S. W.; Fredrickson, G. H.; Kramer, E. J. *Macromolecules* **2003**, *36*, 8712.
(38) Fetters, L. J.; Lohse, D. J.; Richter, D.; Witten, T. A.; Zirkel, A. *Macromolecules* **1994**, *27*, 4639.
(39) Anastasiadis, S. H.; Gancarz, I.; Koberstein, J. T. *Macromolecules* **1988**, *21*, 2980−2987 and references therein.
(40) Khandpur, A. K.; Forster, S.; Bates, F. S.; Hamley, I. W.; Ryan, A. J.; Bras, W.; Almdal, K.; Mortensen, K. *Macromolecules* **1995**, *28*, 8796−8806.
(41) Beyer, F. L.; Gido, S. P.; Velis, G.; Hadjichristidis, N.; Beck Tan, N. *Macromolecules* **1999**, *32*, 6604.
(42) Grason, G. M.; Kamien, R. D. *Macromolecules* **2004**, *37*, 7371.
(43) Bates, F. S.; Schulz, M. F.; Khandpur, A. K.; Forster, S.; Rosedale, J. H.; Almdal, K.; Mortensen, K. *Faraday Discuss.* **1994**, *98*, 7−18.
(44) Matsen, M. W.; Schick, M. *Curr. Opin. Colloid Interface Sci.* **1996**, *1*, 329−336.
(45) Vavasour, J. D.; Whitmore, M. D. *Macromolecules* **1993**, *26*, 7070−7075.
(46) Vavasour, J. D.; Whitmore, M. D. *Macromolecules* **1996**, *29*, 5244−5244.
(47) Mays, J.; Kumar, R.; Sides, S. W.; Goswami, M.; Sumpter, B. G.; Hong, K.; Wu, X.; Russell, T. P.; Gido, S. P.; Avgeropoulos, A.; Tsoukatos, T.; Hadjichristidis, N.; Beyer, F. L. *Polymer* **2012**, *53*, 5155.
(48) Kumar, R.; Sides, S. W.; Goswami, M.; Sumpter, B. G.; Hong, K.; Wu, X.; Russell, T. P.; Gido, S. P.; Misichronis, K.; Rangou, S.; Avgeropoulos, A. T.; Tsoukatos, T.; Hadjichristidis, N.; Beyer, F.; Mays, J. W. *Langmuir* **2013**, *29*, 1995−2006.